Proximate Time-Optimal Reference Tracking of an Undamped Harmonic Oscillator

Roger A. Braker and Lucy Y. Pao

***Abstract*— Motivated by a desire to use compressed sensing in Atomic Force Microscopy, we revisit the Proximate Time-Optimal Servomechanism(PTOSω) regulator we developed previously [15] for the harmonic oscillator, giving a more detailed description of its construction and show new experimental results. Then, we extend that previous work to include set-point tracking. We show that, in contrast to regulator control, the time-optimal switching curve becomes asymmetric, and in fact the problem can be recast as a regulator with asymmetric actuator limits. We then develop a PTOSω approximation and present simulation and experimental results.**

I. INTRODUCTION

The traditional Atomic-Force-Microscope (AFM) imaging method is to raster scan the sample with an atomically sharp probe. Raster scanning is not only a very time consuming process, it can also lead to damaging either the sample or the AFM probe tip or both. Traditionally, efforts to increase imaging speed have focused on increasing the raster scan rate via advanced control algorithms [1], [2].

More recently, researchers have begun to investigate using more efficient scan patterns since often the raster scan spends significant time over uninteresting regions [3]. In a similar vein, [4] suggested a method of AFM imaging whereby a random sample of point-to-point measurements are taken. The sample topology is then reconstructed using the theory of compressed sensing [5]. Taking this random sample of point-to-point measurements reduces the tip-sample interaction and can improve the integrity of both the sample and AFM tip.

Minimizing the imaging time in this scheme requires that the rest-to-rest maneuver times between point measurements be minimized. AFM stages are typically actuated with piezoelectric actuators. The linear dynamics of these actuators are characterized by a series of resonances and anti-resonances which lack of a rigid body mode [6]. This can also be seen in the frequency response of the AFM stage considered in [1]. Hence, even the simplest model for such a stage will be second-order with complex poles. This contrasts with many other mechatronic systems like hard-disk drives which are often reduced to the simplified model of $G(s) = a/s^2$.

For a linear time-invariant system, Pontryagin's Maximal Principle leads to a time-optimal control that is bang-bang [7]. Excellent resources for synthesizing these controls as feedback laws can be found in [8]–[10]. Unfortunately, the bang-bang feedback control is impractical. In any real control system, there will be process and measurement noise, uncertainty in the system parameters and imperfect actuators which will cause the control to chatter between its maximum and minimum values.

A large body of work exists which develops methods to combat this chattering problem. However, much it focuses on rigid body systems. In [11], a robust control law for a double integrator plant is developed using sliding mode techniques. Other researchers have developed the Proximate Time-Optimal Servomechanism (PTOS) for a double integrator plant [12] and a triple integrator plant [13].

Reference [14] suggests pre-computing the time-optimal trajectory which is then tracked with a stabilizing trajectory tracking control law. At the end of this reference trajectory, an end-game control law is implemented to eliminate any final error. A downside to this method is it requires pre-computation of individual trajectories for each initial condition and target state.

In [15], we developed a near time-optimal regulator controller for a system with purely imaginary eigenvalues, which we called the PTOSω. In contrast to the controllers for rigid body plants, this control law is not immediately extendable to set-point tracking. To implement set point tracking for those systems, the switching curve, and hence the PTOS "tube" is simply translated in the phase plane. As we discuss in Section IV, for the simple oscillator system performing reference tracking, not only does the switching curve becomes asymmetric but our control law must be modified to provide a constant input at steady state.

This paper is organized as follows. In Section II we review our previous work with additional details of the method for developing the PTOSω regulator in order to help guide our development of the reference tracking PTOSω. We follow this discussion with some experimental results of the regulator in Section III. We show in Section IV that the time-optimal solution for a holdable set-point is governed by an asymmetric switching curve. We show this curve is a translated copy of the regulator switching curve for a system with asymmetric control limits, which in fact, is the switching curve in the error coordinates. This observation helps us to construct the reference tracking controller as a feedback control law. Using this development, we then extend the PTOSω controller of Section II to the case of set-point tracking in Section V and give a discussion of its stability in Section VI. In Section VI-A, we show experimental results for this set-point tracking PTOSω and provide concluding remarks with a short discussion of the

This work was supported in part by the US National Science Foundation (NSF Grant CMMI-1234980) and Agilent Technologies, Inc.

R.A. Braker is a graduate student and L.Y. Pao is the Richard & Joy Dorf Professor; both are with the Dept. of Electrical, Computer, and Energy Engineering at the University of Colorado, Boulder, CO 80309, roger.braker@colorado.edu, pao@colorado.edu.

case with damping in Section VII.

II. Overview of Regulator PTOSω

Suppose we have a second-order system with imaginary eigenvalues, described in state space by

$$\dot{x} = Ax + Bu(t) \tag{1}$$
$$A = \begin{bmatrix} 0 & 1 \\ -\omega^2 & 0 \end{bmatrix}, \; B = \begin{bmatrix} 0 \\ b_o \end{bmatrix}$$

where the output $y = x_1$ is the position and x_2 is the velocity. It will be useful to define $c = \frac{b_0}{\omega^2}$. The system is driven by a bounded control,[1]

$$u \in [-1, \; +1]. \tag{2}$$

In [15] we modified the time-optimal regulator controller into a near time-optimal regulator, which we called the PTOSω for which we proved stability given an initial state anywhere in $\mathbb{R}^2$. For brevity, here we assume that the initial state is a holdable equilibrium state since ultimately we are interested in rest-to-rest movements. These holdable equilibria are given by $x_{eq} = -A^{-1}Bu$, or, noting (2),

$$x_{2,eq} = 0 \tag{3}$$
$$x_{1,eq} \in [-c, \; +c]. \tag{4}$$

The time-optimal feedback control law is characterized by a switching curve, which is comprised of an infinite sequence of half ellipses. The first set of such ellipses gives the control law as [8]–[10]

$$u = \text{sgn}(f_{to}(x_1) - x_2) \tag{5}$$
$$f_{to}(x_1) = -\text{sgn}(x_1)\omega\sqrt{2c|x_1| - x_1^2}, \;\; |x_1| \le 2c \tag{6}$$
$$\text{sgn}(\xi) = \begin{cases} -1, & \xi < 0 \\ 0, & \xi = 0 \\ +1, & \xi > 0. \end{cases} \tag{7}$$

A. Development of $f_p(x_1)$

Consider the controller given by,

$$u_p(t) = \text{sat}\big[k_2(-x_2 + f_p(x_1))\big]. \tag{8}$$

It will be useful for the ensuing discussions to make use of the following divisions of the state space:

$$\mathcal{T} = \big\{x\colon | - x_2 + f_p(x_1)| \le \frac{1}{k_2}, \quad x_1 \in [-2c, 2c]\big\} \tag{9}$$
$$\mathcal{B} = \big\{x\colon x \in \mathcal{T}, \quad x_1 \in [-c, c]\big\} \tag{10}$$
$$\mathcal{L} = \big\{x\colon x \in B, \quad x_1 \in [-x_\ell, x_\ell]\big\} \tag{11}$$
$$\mathcal{U}^- = \big\{x\colon x \notin \mathcal{T}, \quad x_2 \ge f_p(x_1) + \frac{1}{k_2}\big\} \tag{12}$$
$$\mathcal{U}^+ = \big\{x\colon x \notin \mathcal{T}, \quad x_2 \le f_p(x_1) + \frac{1}{k_2}\big\} \tag{13}$$

[1]It is quite unlikely that a particular system will saturate at ± 1. This convention is made only for convenience here and such systems can be easily dealt with changing b_o to $\bar{b}_o = b_o M$ where M is the new saturation limit.

where $0 < |x_\ell| < c$ and $\mathcal{U}^+$ and $\mathcal{U}^-$ are the regions of the state space which result in a saturated control, while $x \in \mathcal{T}$ results in an unsaturated control and $\mathcal{L} \subset \mathcal{B} \subset \mathcal{T}$.

First, note that a saturator and a gain gives a finite slope approximation to the the sgn$(\cdot)$ function. By making $f_p(x_1)$ approximate $f_{to}(x_1)$ and making k_2 large, then in (8) we an approximation to (5). Furthermore, we can employ a linear feedback controller near the origin (i.e. for $x_1 \in \mathcal{L}$) by defining f_p as the continuously differentiable (for $x_1 \in (-2c, 2c)$) function, defined piecewise as

$$f_p(x_1) = \begin{cases} f_\ell(x_1), & |x_1| \le x_\ell \\ f_{n\ell}(x_1), & x_\ell < |x_1| < 2c \end{cases} \tag{14}$$

where we require that

$$f_\ell(x_\ell) = f_{n\ell}(x_\ell) \tag{15}$$
$$f'_\ell(x_\ell) = f'_{n\ell}(x_\ell). \tag{16}$$

By making $f_\ell(x_1)$ a linear function of x_1, then for $x_1 \in \mathcal{L}$, (8) describes the familiar equation for linear state feedback with the sat$(\cdot)$ function enforcing respect for the control limits. Specifically, define the linear portion of f_p as

$$f_\ell(x_1) \coloneqq -\Big(\frac{k_1}{k_2}\Big)x_1, \quad |x_1| < x_\ell. \tag{17}$$

We construct the entire f_p by connecting this linear f_ℓ to vertical translations of f_{to} so such that (15) and (16) are satisfied. Taking the Taylor approximation of (6) about x_ℓ yields

$$f_{to}(x_1) \approx -\frac{1}{k_2} - \frac{k_1}{k_2}x_1 \tag{18}$$

where

$$k_2 = \frac{\sqrt{2cx_\ell - x_\ell^2}}{\omega c x_\ell} \quad \text{and} \quad k_1 = \frac{c - x_\ell}{c x_\ell}. \tag{19}$$

This is shown as the black curve in Figure 1. Since the switching curve must go through the origin, add the x_2-intercept, $\frac{1}{k_2}$, to (18) to yield $f_\ell(x_1)$, the blue-dashed curve in Figure 1. We connect the parts of f_{to} outside $[-x_\ell, \, x_\ell]$ to f_ℓ by shifting the right portion of f_{to} *up* by $\frac{1}{k_2}$ and the left portion *down* by $\frac{1}{k_2}$. Together, this yields the concatenation of the all the dashed curves in Figure 1. We thus obtain

$$f_\ell(x_1) = -\frac{k_1}{k_2}x_1 \tag{20}$$
$$f_{n\ell}(x_1) = \text{sgn}(x_1)\Big[-\omega\sqrt{2c|x_1| - x_1^2} + \frac{1}{k_2}\Big]. \tag{21}$$

Note that if $x_\ell \to 0$ then $k_2 \to \infty$ and $\frac{1}{k_2} \to 0$ and we recover (5).

Theorem 1: The control law described by (8), (20) and (21) leads to a stable closed loop system.

Proof: For the full proof, see our previous work in [15]. However, the features relevant to this paper are that, provided we restrict $|x_\ell| < 0.4c$: (i) states within region $\mathcal{B}$ remain in $\mathcal{B}$ which we showed by examining the time derivative of $u(t)$ along the upper and lower boundaries of $\mathcal{B}$; and (ii) states in $\mathcal{B}$ tend asymptotically to the origin which we showed by giving a Lyapunov function for region $\mathcal{B}$. ■

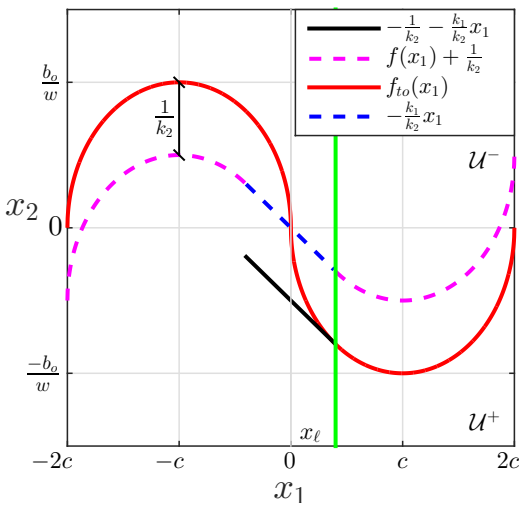

Fig. 1: Illustration of the development of $f_p(x_1)$. The red curve depicts $f_{to}(x_1)$ and the solid black curve is the Taylor approximation of $f_{to}(x_1)$ about x_ℓ. We shift the solid black curve up by $\frac{1}{k_2}$, giving $f_\ell(x_1)$ (dashed-blue). Then, from $[x_\ell,\ 2c]$, we shift f_{to} up by $\frac{1}{k_2}$ and from $[-2c,\ x_\ell]$ we shift f_{to} down by $\frac{1}{k_2}$. This gives f_{ptos} as the concatenation of the dashed curves.

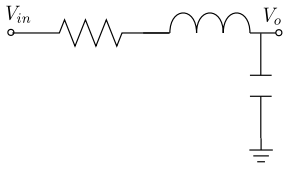

Fig. 2: Schematic of the LRC circuit used to test the control law.

III. Experimental Results

We tested the control law (8) on the LRC circuit shown in Figure 2 which is described by the transfer function

$$\frac{V_o(s)}{V_{in}(s)} = \frac{1/(LC)}{s^2 + \frac{R}{L}s + \frac{1}{LC}}. \tag{22}$$

If we could construct this circuit with $R = 0$, we would have exactly the plant the described in (1). Of course, this is impossible but we can get close. We constructed this circuit with a capacitor and inductor which have the nominal values $C = 0.235\ \mu$F and $L = 100$ mH. The inductor has an internal resistance of $R = 82\ \Omega$. In trying to construct a passive circuit with extremely high Q, note that choosing a larger inductor tends to increases its internal resistance. Of course, we could try to increase $\omega = \sqrt{1/LC}$ by choosing smaller capacitance values and could thus theoretically get arbitrarily low damping. However, since the control law is implemented digitally on an FPGA, this approach is limited by the achievable sample rate. The values chosen represent a compromise between these competing concerns.

We performed a white noise system identification which yielded

$$G(s) = \frac{4.478e7}{s^2 + 743.5s + 4.449e7}. \tag{23}$$

Thus, $\zeta = 0.063$, $\omega = 6669.7$ rad/s, $b_o = 4.478e07$. We programmed the control law in (8) into a National Instruments Compact RIO (NI cRIO-9082) FPGA, using a sample rate of 100 kHz. Because our control law utilizes both states of the system, we implemented a digital prediction observer on the FPGA to provide an estimate of x_2. Since the control law was developed in continuous time, but implemented in discrete time, it is important to ensure that the discrete states of the observer correlate to the continuous time states for fast enough sample rates.

Because the control law utilizes non-linear feedback, analyzing the convergence of the observer and plant becomes problematic. Namely, the separation principle no longer holds. Proceeding anyways, we chose an observer gain $L = [0.440\ \ 4663.6]^T$ which, in the linear case, would place the observer poles at four times the natural frequency of the plant and increase the damping ratio to $\zeta = 0.95$.

We induced an initial condition by issuing a step command of $V_{in} = 1$ volt to the system. After a settling period, we turned on the PTOSω controller. For this experiment we set $x_\ell = 0.1c$. The results of this experiment are displayed in Figures 3 and 4 where it can be seen that even for a plant with small but non-zero damping, our control law performs well, with both the simulation and experiment agreeing nicely.

IV. Reference Tracking Time-Optimal Feedback Controller

Suppose that rather than time-optimal *regulation*, we would like our plant to track *set-point* changes as fast as possible. For plants with imaginary eigenvalues, this new requirement changes the structure of the switching curve, giving it an asymmetry. This is in sharp contrast to rigid body plants where the switching curve is simply shifted in the phase plane. This difference makes set-point tracking in both the time-optimal and PTOSω case more difficult than it is for rigid body plants since the switching curve becomes asymmetric and changes for every new set-point.

To show how this difference comes about, we review the standard derivation of the switching curve [8]–[10]. We minimize the cost

$$J = \int_0^{tf} 1 d\tau \tag{24}$$

which gives the Hamiltonian

$$H = 1 + p^T(Ax + Bu) \tag{25}$$

where $\dot{p} = A^T p$ defines the adjoint dynamics. Given the boundedness of $u(t)$, the minima of H are given by

$$u = -\text{sgn}(p^T B) = -\text{sgn}(p_2(t)b_o). \tag{26}$$

Thus, the control switches at times t_s when the costate $p_2(t)$ vanishes. For the first and last switch, this time is unknown since these roots depend on the boundary conditions for $p(t)$

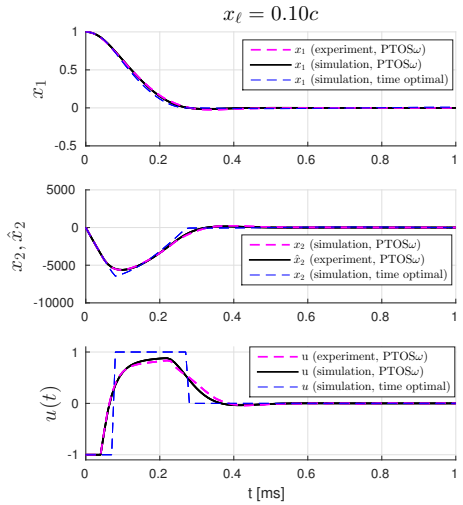

Fig. 3: Comparison between simulation and experimental results for the PTOSω regulator. The controller from both simulation and experiments is driven by the states from a digital observer. Note that in the time series plot of x_2, we have plotted the estimate, $\hat{x}_2$, for the experimental case since this is the only data available.

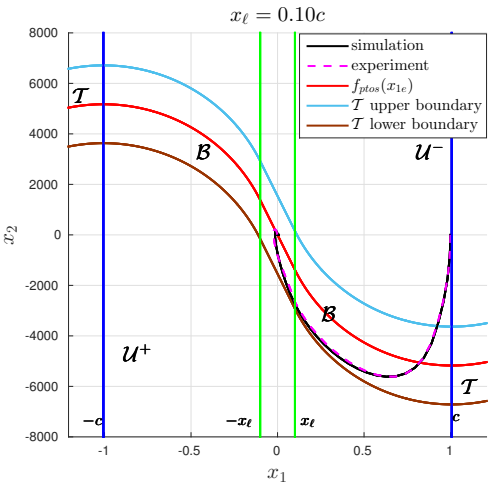

Fig. 4: Phase-plane trajectories of simulated and experimental system.

which are unknown.[2] However we make the observation that, since the costate rotates in its phase plane at a rate of ω, no switch can last longer than π/ω units of time. Thus, we can locate the final leg of any time-optimal trajectory by integrating the system in (1) backwards for π/ω units of time with $u = \pm 1$. This is the curve labeled f_{to} in Figure 1 if $x(t_f) = 0$. Since the control is bang-bang, trajectories approaching this curve must be under the control $u = \mp 1$, and thus the control switches upon the state reaching the curve, prompting us to call it the *the switching curve*. Repeating the process of backwards integration starting from the first segment of f_{to} locates the next segment of the switching curve. However, since the first segments are half ellipses with length $2c$, we need only concentrate on these first segments since we are interested in holdable equilibria, $x_{1eq} \in [-c \;\; c]$.

The typical derivation of the switching curve performs this process beginning at the origin [8]–[10], [16], which yields the regulator of (5). To derive the curve for target states other than the origin, we must integrate backwards starting at the desired reference, x_r. However, to formulate this as a feedback control law, it is more instructive to examine the system in the error coordinates, $x_e = x - x_r$. First, note that when $x_e = 0$, we must apply the constant control

$$u_{ss}(t) = \frac{x_{1r}}{c}, \;\; \forall t \geq t_f \tag{27}$$

if we are to hold the state at x_r. The error dynamics are described by

$$\dot{x}_e = Ax_e + Ax_r + Bu \tag{28}$$

$$= Ax_e + \begin{bmatrix} 0 \\ b_o \end{bmatrix} \left(u - \frac{1}{c} x_{1r} \right). \tag{29}$$

Thus, driving the system to $x(t > t_f) = x_r$ is equivalent to driving the error state x_e to the origin *if the error dynamics are driven by an asymmetric control* $\bar{u}(t)$, namely

$$\bar{u}_{min} = -1 - \frac{1}{c} x_{1r} \tag{30}$$

$$\bar{u}_{max} = 1 - \frac{1}{c} x_{1r}. \tag{31}$$

It will be convenient to refer to (30) and (31) together as $\bar{u}_{\substack{min \\ max}}$. We can construct the time-optimal switching curve for the error coordinates by solving (29) backwards in time from the origin of the error phase plane by integrating

$$x(0) = \bar{u}_{\substack{min \\ max}} \int_T^0 \Phi(0, \tau) B d\tau \tag{32}$$

$$\tag{33}$$

which yields

$$\begin{bmatrix} x_1 \\ x_2 \end{bmatrix} = \begin{bmatrix} \bar{u}_{\substack{min \\ max}} c(1 - \cos \omega(-T)) \\ \bar{u}_{\substack{min \\ max}} \frac{b_o}{\omega} \sin \omega(-T), \end{bmatrix} \tag{34}$$

for $T \leq \pi/\omega$. By eliminating time, we can solve for x_2 as a function of x_{1e} which is $f_{to,e}$,

$$f^-_{to,e} = -\text{sgn}(x_{1e}) \omega \sqrt{2x_{1e} c \bar{u}_{min} - x_{1e}^2}, \;\; x_{1e} < 0 \tag{35}$$

$$f^+_{to,e} = -\text{sgn}(x_{1e}) \omega \sqrt{2x_{1e} c \bar{u}_{max} - x_{1e}^2}, \;\; x_{1e} \geq 0. \tag{36}$$

[2]The difficulty of solving the two-point boundary value problem defined by $\begin{bmatrix} \dot{x} \\ \dot{p} \end{bmatrix} = \begin{bmatrix} Ax + B(-\text{sgn}(p_2 b_o)) \\ A^T p \end{bmatrix}$ arises because (greedily!) $x(t)$ has taken all four boundary conditions and there are none left for $p(t)$.

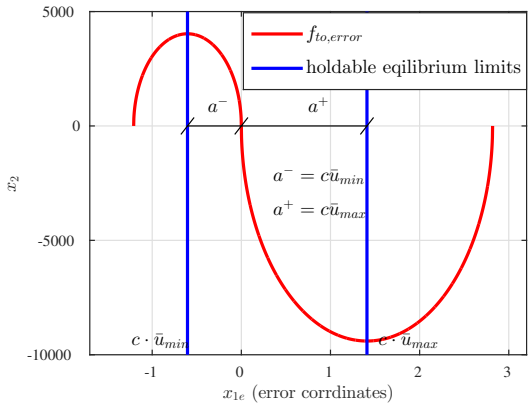

Fig. 5: For target of $x_{1r} = -0.5c$, the plot shows f_{to} in the error coordinates, illustrating the resulting asymmetry

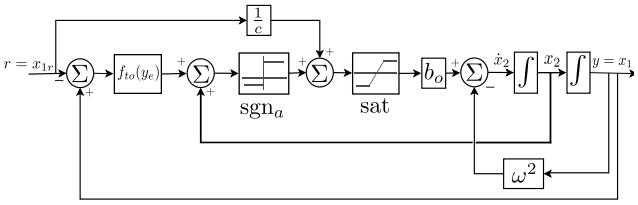

Fig. 6: Block diagram of time-optimal reference tracking controller.

We use the convention that the superscript "$-$" denotes quantities of the left-half phase plane switching curve and "$+$" for the right half phase plane switching curve through the rest of this paper. This switching curve is plotted in Figure 5. It is worth pointing out that the same result, less a translation of x_{1r}, will be obtained by generating the switching curve in the un-shifted coordinates by integrating (1) backwards from x_r.

Note that the ellipse in the negative half-plane is located at center and semi-major axis length of $c\bar{u}_{min}$ while the ellipse in the positive half-plane has center and semi-major axis length of $c\bar{u}_{max}$ so that each ellipse has a different size and a different center. We see then that for reference tracking, the switching curve loses the symmetry of the regulator case.

Though the input to the error dynamics is $\bar{u} \in [\bar{u}_{min}, \bar{u}_{max}]$, the input to the actual plant is still $u \in [-1, +1]$, which we obtain by adding back the required steady-state feedforward input, $u_{ss} = \frac{x_{1r}}{c}$. This development can be implemented as a feedback control law as

$$u = \begin{cases} \text{sgn}_a[f_{to}(x_{1e}) - x_2] + \frac{x_{1r}}{c}, & |x_1| \le 2c \\ \text{sgn}_a(-x_2) + \frac{x_{1r}}{c}, & \text{otherwise} \end{cases} \tag{37}$$

where we define the asymmetric signum is

$$\text{sgn}_a(\xi) = \begin{cases} u_{max}, & \xi > 1 \\ 0, & |\xi| \le 1 \\ u_{min}, & \xi < -1. \end{cases} \tag{38}$$

This control law is illustrated in the block diagram shown in Figure 6. This scheme has the desirable feature that it applies the necessary constant control to hold the state at $x(t) = x_r, \forall\, t \ge t_f$. Note that for the states with $|x_1(0)| > 2c$, the control is not time-optimal. However, since the goal of our control system is to move between steady-state equilibrium points, it is reasonable always to expect that $|x_1| < 2c$ since $\pm c$ is the largest magnitude of a holdable point. The approximation implemented in (37) was suggested in [10] and accounts for the unlikely event this is no longer true.

V. Reference Tracking PTOSω

In a similar vein to the regulator PTOSω, we have developed a PTOS-like controller for the reference tracking situation. Examining Figure 5, the first challenge immediately presents itself. If we are to maintain the continuous differentiability of the PTOS function, which we now call $f_{p,ref}(x_{1e})$, we cannot have $x_\ell^- = x_\ell^+$ since at a single x_ℓ the curves $f_{to,e}^+$ and $f_{to,e}^+$ have different slopes, i.e., $f_{to,e}'^-(x_\ell) \neq f_{to,e}'^+(x_\ell)$. Rather, we need to enforce

$$M = \frac{k_1^-}{k_2^-} = \frac{k_1^+}{k_2^+}. \tag{39}$$

Because the curves are geometrically similar, choosing x_ℓ^- and x_ℓ^+ as a *fraction* of the distance to the center of each ellipse gives us what we need, i.e., for $0 < \lambda \le 1$, choose

$$x_\ell^+ = \lambda c\bar{u}_{max} \tag{40}$$
$$x_\ell^- = \lambda c|\bar{u}_{min}|. \tag{41}$$

We can easily calculate $k_1^\pm$ and $k_2^\pm$ from (19) by replacing c with $\bar{c} = c|\bar{u}_{\substack{min\\max}}|$ and x_ℓ with $x_\ell^\pm$ in (41). Thus, we define $f_{p,ref}$ as

$$f_{p,ref} = \begin{cases} \omega\sqrt{2c\bar{u}_{min}x_{1e} - x_{1e}^2} - \frac{1}{k_2^-}, & -2c < x_{1e} \le -x_\ell^- \\ -Mx_1, & -x_\ell^- < x_{1e} < x_\ell^+ \\ -\left[\omega\sqrt{2c\bar{u}_{max}x_{1e} - x_{1e}^2} - \frac{1}{k_2^+}\right], & x_\ell^+ \le x_{1e} < 2c. \end{cases}$$

The next challenge is in defining the saturation boundaries. In particular, recall that previously, the saturation boundaries were defined by f_p shifted up and down by a factor of $1/k_2$ but now we have *two* different k_2's. It turns out that a reasonable choice is to choose

$$k_2 = \max\left\{k_2^-, k_2^+\right\} \tag{42}$$

and then define the PTOSω reference tracking control as

$$\bar{u}_{p,ref} = \text{sat}_a\left\{k_2[f_{p,ref} - x_2]\right\} \tag{43}$$

where the asymmetric saturator is given by

$$\text{sat}_a(\xi) = \begin{cases} \bar{u}_{max}, & \xi > \bar{u}_{max} \\ \xi, & \bar{u}_{min} \le \xi \le \bar{u}_{max} \\ \bar{u}_{min}, & \xi < \bar{u}_{min}. \end{cases} \tag{44}$$

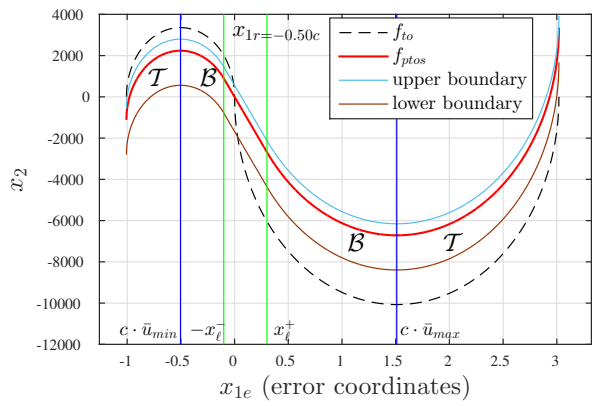

Fig. 7: Set-point tracking $f_{p,ref}$ curves and saturation region

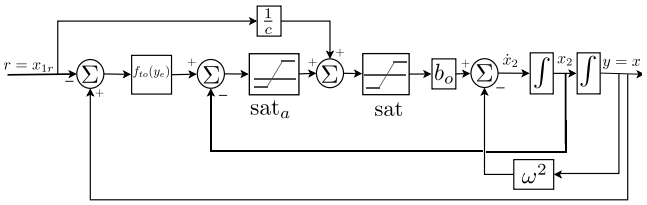

Fig. 8: Block diagram of the PTOSω reference tracking controller.

This gives the saturation boundaries as

$$x_2^{upper} = f_{p,ref}(x_1) - \frac{\bar{u}_{min}}{k_2} \tag{45}$$

$$x_2^{lower} = f_{p,ref}(x_1) - \frac{\bar{u}_{max}}{k_2} \tag{46}$$

which is shown in Figure 7. Just as in the time-optimal case, for use in the regular coordinates, we add back the required steady-state feedforward control which yields

$$u_{p,ref} = \text{sat}_a \left\{ k_2 [f_{p,ref} - x_2] \right\} + \frac{x_{1r}}{c}. \tag{47}$$

This control law can be implemented according to the block diagram of Figure 8.

VI. Stability of the Reference Tracking PTOS

A generalized stability analysis has yet to be done. However, if we consider the plant in (23), it is straightforward to show using the techniques we described in [15] that for a *particular* choice of x_{1r} and λ (i.e., x_ℓ), we have a stable closed-loop system. For the simulations in the next section, we will use $x_{1r} = -0.5c$ and $\lambda = 0.1$. To see that $x_e \in \mathcal{B}$ does not exit via the saturation boundaries, we consider the time derivative of $u_{p,ref}(t)$ along the boundaries of $\mathcal{B}$ which is

$$\dot{u}_{p,ref} = f'_{p,ref}(x_{1e}) \underset{max}{\bar{u}_{min}} + k_2 f'_{p,ref}(x_{1e}) f_{p,ref}(x_{1e}) + k_2 \omega^2 x_{1e} - k_2 b_o \underset{max}{\bar{u}_{min}} \tag{48}$$

where $\dot{u}_{p,ref} > 0$ along the upper boundary and $\dot{u}_{p,ref} < 0$ along the lower boundary implies that the state does not exit.

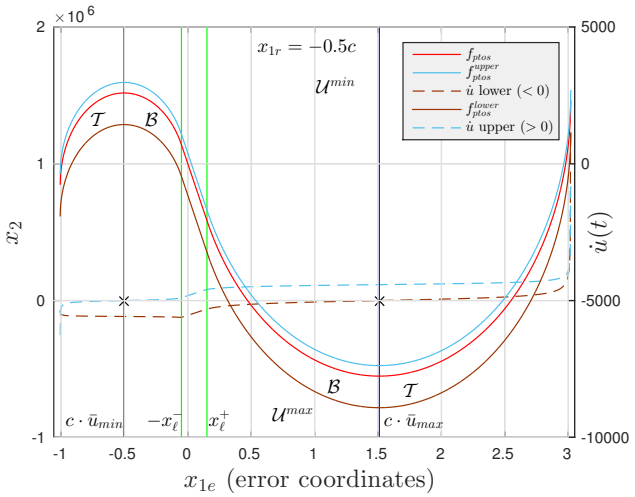

Fig. 9: This figure shows $\dot{u}$ evaluated along the upper and lower saturation boundaries, for $x_{1r} = -0.4c$ and $\lambda = 0.1$. Since for the state to remain trapped in $\mathcal{B}$, we need $\dot{u}_{p,ref} < 0$ along the lower boundary and $\dot{u}_{p,ref} > 0$ along the upper boundary, this plot shows $\mathcal{B}$ is invariant.

Using these parameters and a forward difference approximation to calculate $f'_{p,ref}$, we can plot (48) evaluated along both the upper and lower boundaries. This is shown in Figure 9. Indeed, we see that $\dot{u}_{p,ref}$ evaluated at the upper boundary becomes negative at $c\bar{u}_{min}$. Similarly, $\dot{u}_{p,ref}$ evaluated along the lower boundary becomes positive at $c\bar{u}_{max}$ which indicates that a state $x_e \in \mathcal{B}$ remains in $\mathcal{B}$. To see that $x_e \in \mathcal{B}$ tends asymptotically to the origin (of the error space), we use the Lyapunov function

$$V(x_e) := \frac{1}{2} x_2^2 + \int_0^{x_{1e}} p(s) ds \tag{49}$$

$$p(x_1) := \omega^2 x_{1e} - b_o k_2 f_{p,ref}(x_{1e}). \tag{50}$$

This is nearly the same Lyapunov function we used in [15] aside from a sign difference that accounts for the definition of $f_{p,ref}$ differing by a negative sign. The positive definiteness of $V(x)$ and negative definiteness of $\dot{V}(x)$ follow from the arguments given in that work with the following modification. Rather than appealing to the symmetry of $f_{p,ref}$, (which is now lacking), we note from Figure 7 that

$$f_{p,ref} < 0, \quad 0 < x_{1e} < c\bar{u}_{max} \tag{51}$$

$$f_{p,ref} > 0, \quad c\bar{u}_{min} > x_{1e} > 0. \tag{52}$$

$$\tag{53}$$

Thus, the integral, $\int_0^{x_{1e}} f_{p,ref}(s) ds$ always yields a negative area so that (49) is still positive definite.

A. Reference tracking PTOSω results

Using the same experimental setup as discussed in Section III, we tested the reference tracking PTOSω controller. The time histories of these results are shown in Figure 10 along with the simulated time-optimal trajectories for comparison. Figure 11 shows the phase-plane plots for the

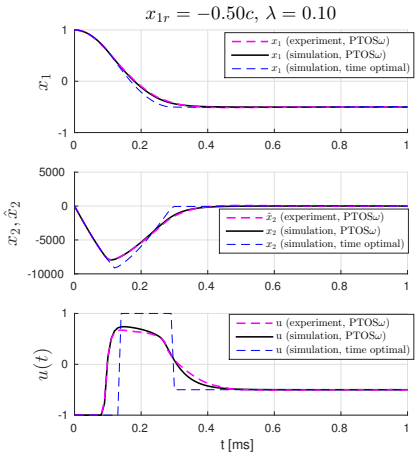

Fig. 10: Comparison between simulation and experimental results for the reference tracking PTOSω. The initial condition is set to $x_1 = 1$ and the reference is $x_{1r} = -0.5c$. The controller from both simulation and experiments is driven by the states from a digital observer. Note that in the time series plot of x_2, we have plotted the estimate, $\hat{x}_2$, for the experimental case since this is the only data available.

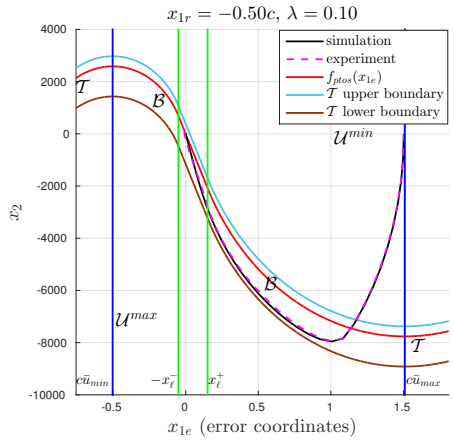

Fig. 11: Phase-plane trajectories in the error coordinates of both the simulated and experimental systems.

simulated and experimental systems. As predicted above, the states do indeed remain trapped in $\mathcal{B}$.

VII. Conclusions And Remarks on Damping

In this paper, we have given a detailed derivation of the PTOSω which we then extend to include reference tracking. We also verified these controllers in both simulation and physical experiment on an LRC circuit. While we have argued the stability of the reference tracking PTOSω controller based upon our previous stability proof of the PTOSω regulator, a rigorous stability proof for the tracking controller is still an area of future work.

To properly include damping will be significantly more challenging. The switching curve in that case is described by a logarithmic spiral. Though it is still possible to eliminate time from the equations as we did with (34), it is not possible to isolate x_1 or x_2 on one side. Nonetheless, the switching curve is easily generated via backwards integration and can then be represented in a lookup-table. The techniques discussed in Sections II-A and V can be used to create a "numeric" PTOSω controller, e.g., by numerically calculating the derivatives of f_{to} to generate $k_1^{\pm}$ and $k_2^{\pm}$. Challenges still exist, however, since f_{to} is represented in a lookup-table and f_{to} changes for every reference input. For our use-case, of visiting a pre-determined set of points for a compressed sensing scheme, it is also possible to generate a family of switching curves offline and then program the controller to download the next needed curve while the current set point is being tracked.

References

[1] J. Butterworth, L. Y. Pao, and D. Abramovitch, "Dual-adaptive feedforward control for raster tracking with applications to AFMs," in *Control Applications (CCA), IEEE International Conference on*, Sep. 2011, pp. 1081–1087.

[2] S. Salapaka, A. Sebastian, J. P. Cleveland, and M. V. Salapaka, "High bandwidth nano-positioner: A robust control approach," *Review of Scientific Instruments*, vol. 73, no. 9, pp. 3232–3241, 2002.

[3] J. Worthey and S. Andersson, "Local circular scanning for autonomous feature tracking in AFM," in *American Control Conference (ACC)*, July 2015, pp. 3490–3495.

[4] S. Andersson and L. Pao, "Non-raster sampling in atomic force microscopy: A compressed sensing approach," in *American Control Conference (ACC)*, June 2012, pp. 2485–2490.

[5] E. Candes and M. Wakin, "An introduction to compressive sampling," *Signal Processing Magazine, IEEE*, vol. 25, no. 2, pp. 21–30, Mar. 2008.

[6] H. Adriaens, W. De Koning, and R. Banning, "Modeling piezoelectric actuators," *Mechatronics, IEEE/ASME Transactions on*, vol. 5, no. 4, pp. 331–341, Dec. 2000.

[7] A. Bryson and Y. Ho, *Applied Optimal Control*. Hemisphere Publishing Corporation, 1975.

[8] E. P. Ryan, *Optimal Relay and Saturating Control System Synthesis*. Peter Peregrinus, 1982.

[9] R. Oldenburger and G. Thompson, "Introduction to time optimal control of stationary linear systems," *Automatica*, vol. 1, no. 23, pp. 177 – 205, 1963.

[10] M. Athans and P. L. Falb, *Optimal Control*. Mineola, New York: Dover Publications, Inc., 2007.

[11] W. Newman, "Robust near time-optimal control," *Automatic Control, IEEE Transactions on*, vol. 35, no. 7, pp. 841–844, Jul. 1990.

[12] M. Workman, "Adaptive Proximate Time-Optimal Servomechanisms," Ph.D. dissertation, Stanford University, Stanford, CA, Mar. 1987.

[13] L. Pao and G. Franklin, "Proximate time-optimal control of third-order servomechanisms," *Automatic Control, IEEE Transactions on*, vol. 38, no. 4, pp. 560–580, Apr. 1993.

[14] J. L. Junkins and Y. Kim, *Introduction to Dynamics and Control of Flexible Structures*. Washington, DC: American Institute of Aeronautics and Astronautics, Inc., 1993.

[15] R. A. Braker and L. Y. Pao, "Proximate time-optimal control of a second-order flexible structure," *IEEE Conference on Control Applications (CCA), part of IEEE Multi-Conference on Systems and Control*, pp. 840–845, Sept. 2015.

[16] I. Flugge-Lotz, *Discontinuous and Optimal Control*. New York, New York: McGraw-Hill Book Company, 1968.